Isenburg, K., Liu, Y., Morin, T.M., & Stern, C.E. (2026). Connectome Fingerprinting Predicts Prefrontal Cortical Activation During Abstract Reasoning. *Imaging Neuroscience*, Advance Publication. https://doi.org/10.1162/IMAG.a.1460

Connectome Fingerprinting Predicts Prefrontal Cortical Activation During Abstract Reasoning

Kylie Isenburg[1,2*], Yixiang Liu[2,4*], Thomas M. Morin[2,3], Chantal E. Stern[1,2,4]

[1]Graduate Program for Neuroscience, Boston University, 02215

[2]Cognitive Neuroimaging Center, Boston University, 02215

[3]Department of Radiology, Massachusetts General Hospital, 02129

[4]Department of Psychological and Brain Sciences, Boston University, 02215

Author Note

Correspondence regarding this article should be addressed to Chantal Stern, Department of Psychological and Brain Sciences, Boston University, Boston, Massachusetts, 02215. Email: chantal@bu.edu Phone: 617-353-1396

* This manuscript has shared first authorship.

Key Words: Neuroimaging, Connectome, fMRI, Cognition, Connectivity

© 2026 The Authors. Published under a Creative Commons Attribution 4.0 International (CC BY 4.0) license.

Abstract

Connectome fingerprinting (CF) is a machine learning technique that uses an individual's unique brain connectivity profile to make predictions about their individual brain activity patterns. Previous studies have successfully employed CF using sensory, working memory, and auditory/visual fMRI data. Here, we demonstrate that this technique can be used to examine higher-order cognition and evaluate the effectiveness of the CF method in the prefrontal cortex (PFC), an area where brain function and structure has been shown to be exceptionally variable across individuals. We designed a CF model, using a leave-one-out cross-validation scheme, to predict individually-specific blood-oxygen-level-dependent (BOLD) activation in the lateral PFC. We used an abstract reasoning task designed to probe higher-order cognitive function specific to the lateral PFC. Our results demonstrated that CF better predicts abstract reasoning activation in the lateral PFC compared to the group average. We also tested whether task-evoked BOLD activity could be predicted using a model trained on a subset of the functional connectome. We demonstrate that CF models trained on a partial connectome from associative brain networks achieved similar levels of model performance compared to models trained on the full connectome. We observed that model performance varied across participants, suggesting that within-participant reliability in task activation, and deviation from the group average influence the model. Overall, we used CF to characterize individuals' task-evoked BOLD activation during abstract reasoning, demonstrating a link

between resting-state functional architecture and brain activations and identifying key networks that contribute to higher-order cognition.

1. Introduction

Brain activity patterns measured with functional magnetic resonance imaging (fMRI) can be highly variable at the individual level. This variability is amplified by the low signal-to-noise ratio and often small sample sizes (Gordon et al., 2017; Welvaert & Rosseel, 2013). In fact, successful functional precision mapping has required the aggregation of hours of resting-state data from one person across many sessions (Ooi et al., 2025), making this infeasible in a large-scale cohort. While group averaging improves the statistical reliability of blood oxygen level dependent (BOLD) activation, it can also have the effect of obscuring meaningful differences. A growing body of research has emphasized the importance of considering individual variability in fMRI activation (Amunts et al., 2000; Bürgel et al., 2006; Mangin et al., 2004; Mueller et al., 2013), asserting that group averaging glosses over cognitively meaningful information and blurs the fine-scale organization of interdigitated brain networks (Braga & Buckner, 2017; Buckner & DiNicola, 2019; DiNicola et al., 2023; Somers et al., 2021; Specht, 2020). Further, these individual differences make network models challenging to define, as they can depend on both state (task-dependent) and/or trait (participant-dependent) components that are difficult to differentiate from model noise (Bassett et al., 2018). This is of particular concern in the prefrontal cortex (PFC), a brain region at the core of many higher-order cognitive tasks, with known individual structural (Rajkowska & Goldman-Rakic, 1995) and functional variation(Mueller et al., 2013).

Machine learning approaches, including Connectome Fingerprinting (CF), have been used to offer a more detailed view of individual-level BOLD activation. CF uses an individual's

brain connectivity profile (e.g. functional connectome) to predict information about activity patterns or cognitive performance, akin to a unique "fingerprint" (Passingham et al., 2002). CF has a broad range of applications. For example, in a hallmark study by Finn et al. (2015), whole-brain functional connectomes were used to demonstrate that each participant's functional connectome at session one was predictive of their subsequent functional connectomes (Finn et al., 2015). The technique has also been used to predict evoked BOLD activation during sensory and perceptual tasks (Amico & Goñi, 2018; Finn et al., 2015; Mars et al., 2018; Osher et al., 2019; Tobyne et al., 2018; Tripathi et al., 2024; Tripathi & Somers, 2023), to predict behavioral outcomes (Shen et al., 2017), to predict symptoms of attention disorders (Rosenberg et al., 2015, 2016), and in place of functional localizers to identify regions of interest (ROIs) along the ventral visual stream (Molloy et al., 2024).

In addition to its practical applications, CF may offer theoretical insight into the relationships between task-based BOLD activation and an individual's underlying functional network architecture. In the original "Connectome Fingerprinting" paper by Passingham and colleagues, it is argued that each cortical area of the brain has a fingerprint of connections, and that these connections underly the observed neuronal activation patterns across various tasks (Passingham et al., 2002). This would suggest that task-activation patterns hold, at least partially, non-variable trait-level information. A recent paper investigating the relationship between resting-state functional connectivity and task activations across 33 cognitive domains supports this idea, finding tight coupling between the average whole-brain connectivity matrix and all 33 unique cognitive domains (Hiersche et al., 2026). Further, resting-state

network stability has been replicated across datasets, tasks, and individual participants (Braga & Buckner, 2017; Cole et al., 2014; Gratton et al., 2018; Kraus et al., 2021; Power et al., 2011; Thomas Yeo et al., 2011). There is also evidence that some amount of flexible reconfiguration of specific networks is necessary for specific cognitive functions (Liao et al., 2017; Mattar et al., 2018; Morin et al., 2023). Importantly, despite clear relationships between the functional connectome and task activations at the group level, participant-specific differences in network topology influence the inter-individual variability in task activation patterns (Chan et al., 2017).

In this study, our goal was to extend the use of the CF technique to an abstract reasoning task to address two questions: 1) how much information in individual-level activation patterns can be linked to idiosyncratic functional network architecture?, and 2) what is the capacity of the CF method in capturing this link during a higher-order cognitive task? Abstract reasoning is a goal-oriented process whereby rules of a specific context are identified and applied to novel situations. fMRI research has implicated the PFC as having a key role in abstract reasoning (Hasselmo & Stern, 2018; Hoshi et al., 2000; Mansouri et al., 2020; Miller & Cohen, 2001; Morin et al., 2023; Wallis et al., 2001). The lateral PFC shows increased BOLD activation during abstract reasoning tasks (Melrose et al., 2007, 2018; Prabhakaran et al., 1997; Shin & Jeon, 2021) and functional reconfiguration when transitioning from resting-state into an abstract-reasoning task-state (Hearne et al., 2016; Morin et al., 2023). Higher-order cognitive brain activity is highly variable in the lateral PFC (Buckner & DiNicola, 2019; DiNicola et al.,

2023), and employing CF during an abstract reasoning task offers a unique opportunity to assess the level of trait-specific task-relevant information held in multi-modal brain networks at rest.

In this study, we employed a cross-validated leave-one-out ridge regression technique (LOOCV) on functional connectomes generated from resting-state fMRI data to predict lateral PFC activation during a simplified version of the Raven's Progressive Matrices (RPMS) reasoning task (Morin et al., 2023; Raven, 1941). We hypothesized that a CF model would be more accurate than that of the group average benchmark. Moreover, given previous findings that associative networks, particularly the frontoparietal network, showed higher predictive weights, (Finn et al., 2015; Peña-Gómez et al., 2018), we hypothesized that a subset of the networks would be sufficient for good model performance. We tested this by splitting the connectome into subsets, namely association-related and sensory-related connectomes. Finally, we identified factors that may influence our model performance, including within-individual variation in task activity and deviation from the group average.

Results of this study demonstrate that LOOCV CF can be successfully employed during a higher-order cognitive task, in our case abstract reasoning, in an individually variable brain region such as the lateral PFC. Our CF model was better able to predict individual-participant BOLD activation compared to the group average. In addition, we identified a subset of associative brain networks that combine into a functional connectome which performs as efficiently as the whole-brain connectome for predicting task activation. This suggests that the underlying functional architecture of these networks partially shapes BOLD activation

patterns during higher-order cognition. Thus, trait-specific information present at rest is also a highly relevant feature of state-level task activation in higher-order cognition.

2. Methods

2.1 Participants

We re-analyzed an existing dataset of 31 healthy participants who were recruited from Boston University and the greater Boston area (Morin et al., 2023). All participants had normal or corrected to normal vision and no history or current diagnosis of neurological or psychiatric disorders. 23 participants were included in the final analysis (19-34 years of age (mean: 26), 14 female). We excluded 1 participant due to low accuracy on the behavioral task (<80% in at least one condition), 3 due to excessive head motion (>3 mm framewise displacement (FD) during at least 2 TRs within a single scan run (uninterrupted acquisition period of a task)), and 4 for not having enough resting-state data for the present analysis. The mean FD across all participants and scans as 0.12mm, indicating extremely low overall head motion aside from the 3 excluded participants. All participants gave written informed consent in accordance with Boston University's Institutional Review Board and were compensated for their time.

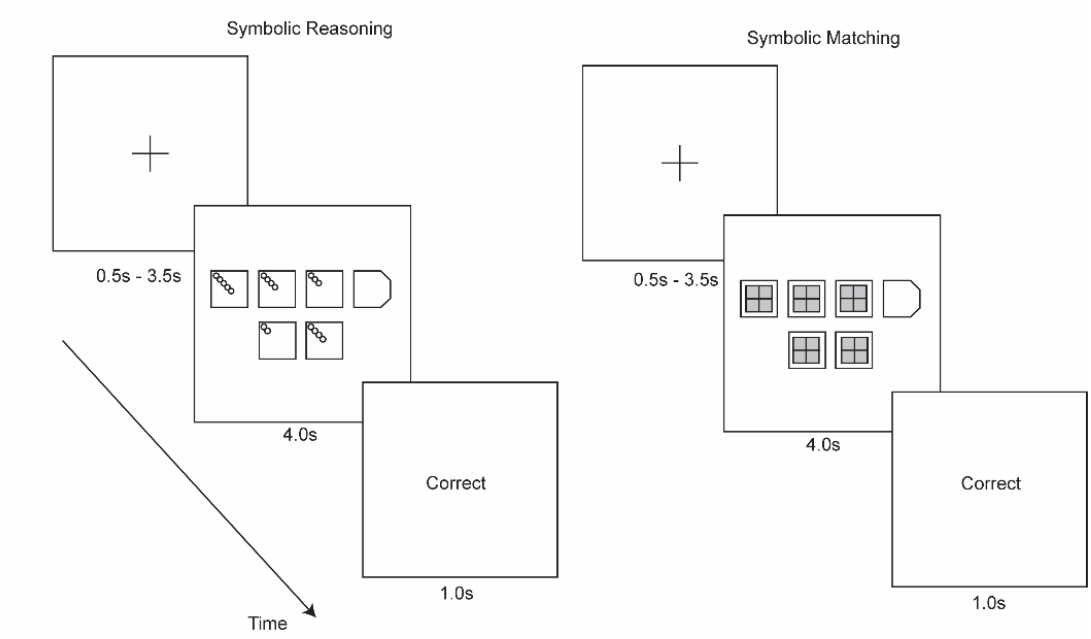
2.2 Experimental Design

During fMRI scanning, all participants performed an in-scanner version of the RPMS (RAVEN, 1941). The present analyses included two conditions: one experimental and one control (**Figure 1**). The experimental condition was designed to investigate abstract reasoning

ability via a symbolic reasoning task. In this condition, participants were asked to look at a series of discrete symbols that followed a sequential rule from left to right. For each trial, participants were shown the stimulus with two potential answer choices, followed by a 4.0 s time-window where they were to determine the answer-choice that best fit the sequential pattern. They were then given feedback as to whether it was a 'Correct', 'Wrong', or 'No Response' trial (1.0s). For the control condition, the symbolic sequences were also coupled with 'matching' trials. In this condition, participants were shown discrete images of the same symbol, and determined which answer-choice was an identical match to the stimulus. Participants completed a total of 384 trials, 96 of each condition. A detailed description of the task design, implementation, and timing can be found in Morin et al., 2023.

2.3 MRI Data Acquisition

Figure 1



RPMS Task design. We utilized fMRI data from a previous study in our lab (Morin et al., 2023) that employed a simplified version of the Raven's Progressive Matrices task shown here. The experimental condition of interest was 'Symbolic Reasoning' whereby a sequentially changing patterns of symbols was shown followed by two potential answer choices for the participant to choose from. This condition was contrasted with a 'Symbolic Matching' control where the participant saw sequentially matching patterns and had to select the match between two answer choices.

MRI data were collected using a 3 Tesla Siemens MAGNETOM Prisma MR scanner located in the Cognitive Neuroimaging Center at Boston University in Boston, Massachusetts. Data were acquired using a 64-channel head coil. Each subject underwent a T1-weighted MEMPRAGE RMS structural scan (TR = 2200 ms, TE = 1.67, Flip Angle=7°, Resolution = 1 mm isotropic) and three runs of T2*-weighted echo-planar (BOLD) resting-state functional MRI (multiband sequence, slice acceleration factor of 6, TR = 1000ms, TE=30ms, Flip Angle = 60°). For each resting-state acquisition, subjects were asked to lie still and fixate on a crosshair on the screen displayed in front of them for 6 minutes. For task scan runs, T2*-weighted echo-

planar (BOLD) images were acquired (multiband sequence, slice acceleration factor of 3, TR = 2000, TE = 30ms, Flip Angle = 60°, partial-fourier acquisition). All functional runs were composed of 78, whole-brain slices with a voxel-size of 2 mm isotropic. Further, two opposite phase-encoding EPI fieldmaps were acquired for each subject for distortion correction (TR=8540 ms, TE = 66 ms, Flip Angle = 90°).

2.4 Data Preprocessing & Lower-Level General Linear Models

All data were preprocessed using the standardized pipeline available in fMRIprep (v1.4.1) (Esteban et al., 2019). The steps included skull stripping, fieldmap distortion correction, co-registration of participant-specific functional data to their anatomical images using boundary-based registration with 12 degrees of freedom, head-motion estimation, slice-timing correction, non-linear transformation of anatomical and functional data to a standard template space (MNI152NLin2009cAsym), and projection onto a standardized cortical surface (fsaverage). Following preprocessing, we spatially smoothed the data with a Gaussian kernel (3mm FWHM). Full details of fMRIprep's pipeline can be found in the Supplementary Materials Section 1.

First level voxelwise general linear models (GLMs) were performed in surface space on single-participant data using Freesurfer's FsFast. Regressors included boxcar regressors convolved with a gammafit hemodynamic response function (alpha = 2.25, beta = 1.25) to model the task conditions, a second order polynomial to account for linear and quadratic trends, and six motion-related nuisance regressors to account for translation and rotation in

185 the x, y, and z directions. The resulting z-statistic maps were generated on the concatenation
186 of all first level runs.
187
188 *2.5 Search Space Selection*
189 The lateral PFC is important for abstract reasoning tasks, specifically those requiring
190 relational integration (Christoff et al., 2001; Golde et al., 2010; Green et al., 2012; Prabhakaran
191 et al., 1997).In our previous study, we found increased activity of the lateral PFC associated
192 with abstract reasoning (Morin et al., 2023). Moreover, when contrasting the symbolic
193 condition with a separate experimental condition that utilized continuous rather than discrete
194 patterns, large clusters of lateral PFC activation remained. This activity fell within the
195 boundaries of the previously defined Yeo-7 parcels of the cognitive control network (CCN)
196 (Thomas Yeo et al., 2011), a network of frontoparietal regions commonly associated with
197 higher-order cognition. Using the Schaefer 400-parcellation of the Yeo 7 Networks we defined
198 a search space consisting of 6,110 vertices in the left hemisphere and 10,945 vertices in the
199 right hemisphere that make up areas of lateral PFC delineated by the CCN (Schaefer et al.,
200 2018; Yeo et al., 2011).
201
202 *2.6 Individual Functional Connectomes*
203 For each participant, whole-brain individual functional connectomes were constructed
204 for both hemispheric search spaces. In each hemisphere, the time-series of the vertices within
205 each parcel of the Schaefer-400 atlas (with the exception of search space vertices) were

averaged to create a parcel-specific time-series. The parcel data was then correlated with the time-series data from each vertex within the search space, thus creating two vertex-to-parcel functional connectomes, one for each hemisphere.

In order to investigate whether whole-brain connectomes are necessary for accurate ridge predictions, we split the connectivity matrices in two: one included nodes in unimodal sensory networks and the other included nodes in multimodal associative networks. The sensory functional connectome was composed of nodes from the visual, limbic, and somatomotor networks of the Schaefer 400-atlas. The associative functional connectome was composed of nodes from the default mode, dorsal attention, ventral attention, and cognitive control networks (Schaefer et al., 2018; Thomas Yeo et al., 2011). Both connectomes were constructed for each hemisphere with the same vertex-to-parcel method used for the whole-brain analysis.

As a validation for our split connectivity matrices, we also extracted whole-brain model coefficients and averaged them across participants. These coefficients were then plotted on the brain in heatmap colors indicating a gradient of weakest to strongest model weights from each parcel to the lateral PFC search space in both hemispheres. This allowed us to examine whether the parcels contributing the most to the whole-brain CF model overlapped with either of our sub-network models.

2.7 Training Procedures and Ridge Regression Predictions

Consistent with previous research (Osher et al., 2019; Smittenaar et al., 2017; Tobyne et al., 2018; Tripathi & Somers, 2023; Wang et al., 2017), this study employed ridge regression (Hoerl & Kennard, 1970) using a nested LOOCV (Hastie et al., 2009). The regression was modeled based on L2-regularized linear regression, shown below.

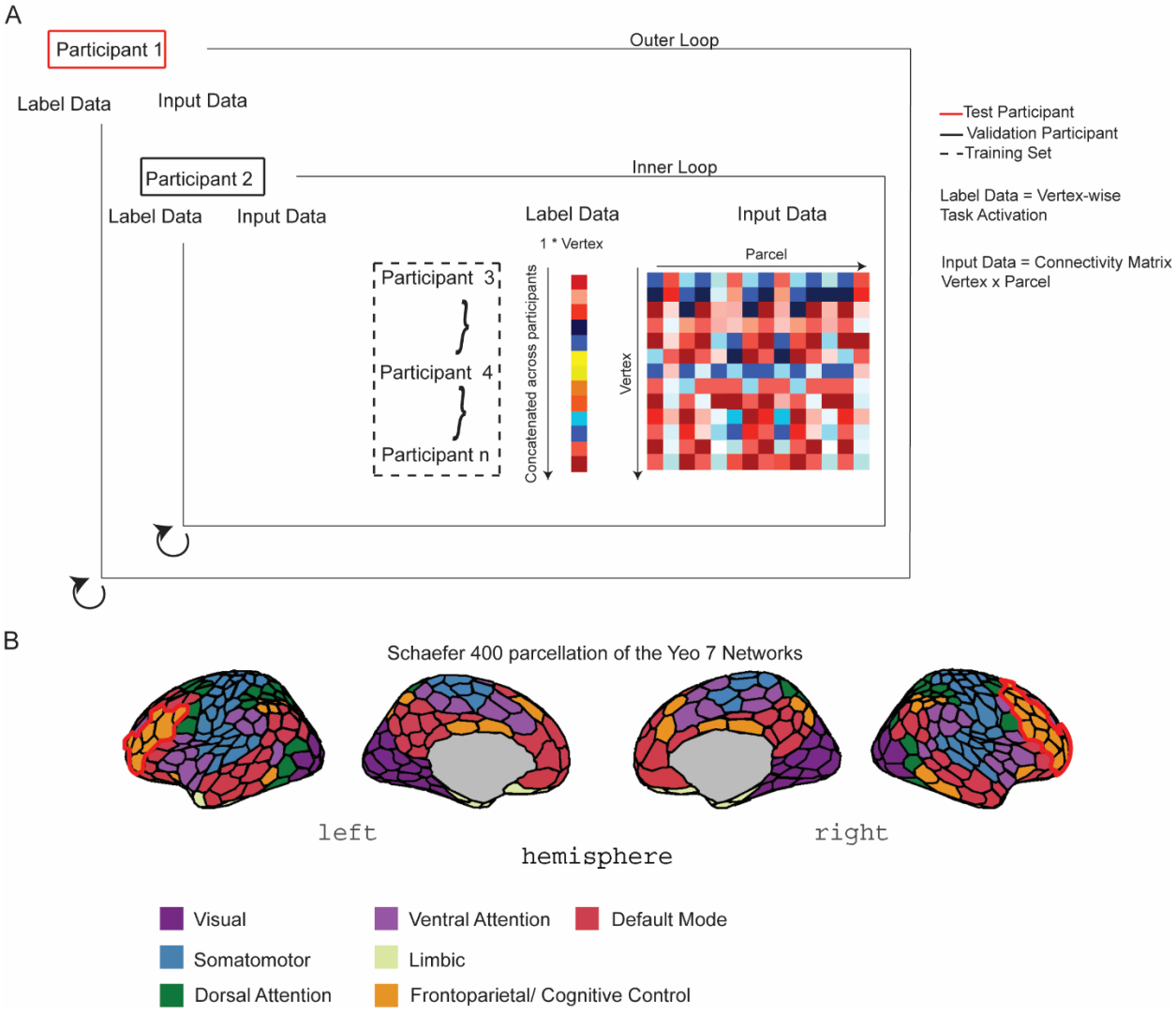
$$\left(\hat{\beta}_0, \hat{\beta}\right) = \operatorname{argmin}_{\beta_0,\beta} \sum_{i=1}^{n} (y_i - \beta_0 - \sum_{j=1}^{p} \beta_j x_{i,j})^2 + \underbrace{\lambda \sum_{j=1}^{p} \beta_j^2}_{Penalty}$$

Here, the estimated intercept $\hat{\beta}_0$ and coefficient $\hat{\beta}$ are chosen to minimize the residual sum of squares, measuring how far our model prediction is from true individual task activation (y) at vertex i, for all vertices up to n. In this model, B_j represents the inferred coefficients associated with connectivity profile X (functional connectivity between vertex i and parcel j), p is the total number of model features, and $\lambda \geq 0$ is the ridge regularization hyperparameter that determines the penalty strength on the estimated parameters. This penalty term is important for ensuring smaller, more stable coefficients that prevent overfitting to the training set.

This LOOCV procedure involved two parallel steps: an 'outer loop' and a nested 'inner loop', in order to optimize hyperparameter values for the left-out participant. For each iteration of the outer loop, a single participant was removed from the model as the test data for that loop. The remaining n-1 participants were then passed to the nested inner loop where another participant was removed for model training validation. The model was then trained

on the BOLD activation values within the search space utilizing the concatenated functional connectomes of these n-2 participants. Within the nested inner-loop, we applied a grid-search strategy to evaluate 100 regularization hyperparameter values λ over a range of 10^0 to 10^7. An optimal model was set as that which generated the lowest mean squared error across all models. This process was iterated n-1 times, leaving each inner-loop participant out once as a validation. The optimal λ was then calculated by averaging across the resulting best fitting models of the inner loop. This model was subsequently used to train the outer loop functional connectomes to predict the BOLD activation values of the left-out participant, repeated n times (**Figure 2**). We computed ridge regression predictions using the whole-brain, sensory, and association functional connectomes separately. This resulted in three different ridge predictions for each hemisphere based on the connectome that the model was trained on.

Figure 2



Method for LOOCV. Example for one loop of the model completed on test 'Participant 1'. The outer loop and nested inner loop of the model are denoted by solid black lines.The label and input data for the test subject outlined in red are left out in the outer loop. All n-1 subjects are funneled into the inner loop whereby 'Participant 2' outlined in black is then left out as the validation subject. The inner loop label data represents task activation across each vertex, concatenated by row across training-level participants. The inner loop input data represents connectivity matrices made up of vertex x parcel connectivity, concatenated by row across training-level participants. The model is trained on the label data of the n-2 remaining participants utilizing their input data. An optimal hyperparameter value is chosen that best fits the model. The validation participant is iterated through all nested inner-loops and the optimal hyperparameter values are then averaged and fit to the test participant. This is repeated n times. B) The Schaefer 400 parcellation of the Yeo 7 networks. The search space for the present analysis is outlined in red.

2.8 Group average benchmark & null distribution comparison

To assess the performance of the LOOCV predictions, we also established a group average benchmark constructed using a leave-one-out group mean (LOOGM) approach. In this approach, we excluded one participant at a time. During each iteration, we concatenated the first-level activation maps across all n-1 participants and fit a GLM to calculate the average group-level value at each vertex. This created out one-sample group mean maps for each left-out participant. We then calculated a voxelwise correlation between the left-out participant's first-level activation results and the LOOGM results. The correlation coefficients were Fisher's z-transformed for later analysis against the LOOCV model.

As an additional control analysis, we calculated participant-specific null models to assess meaningful spatial structure beyond chance. For each participant's search space, we randomly permuted the model's vertex-wise predicted activation values 1000 times, calculating a Pearson's correlation coefficient between the new shuffled values and the true vertex-wise values at each iteration. This model yields a null distribution that would be expected under the null hypothesis of a random spatial structure. We then calculated a p-value by computing the proportion of newly permuted correlations that were equal to or greater than the original model's observed values, to test whether the predictions held spatially meaningful specificity. We did this for each of our CF models in both hemispheres.

2.9 Statistical Analysis of Ridge Model Performance

To calculate model performance, participant-specific predicted activation values were correlated with the first level GLM BOLD values, leaving each participant with a model

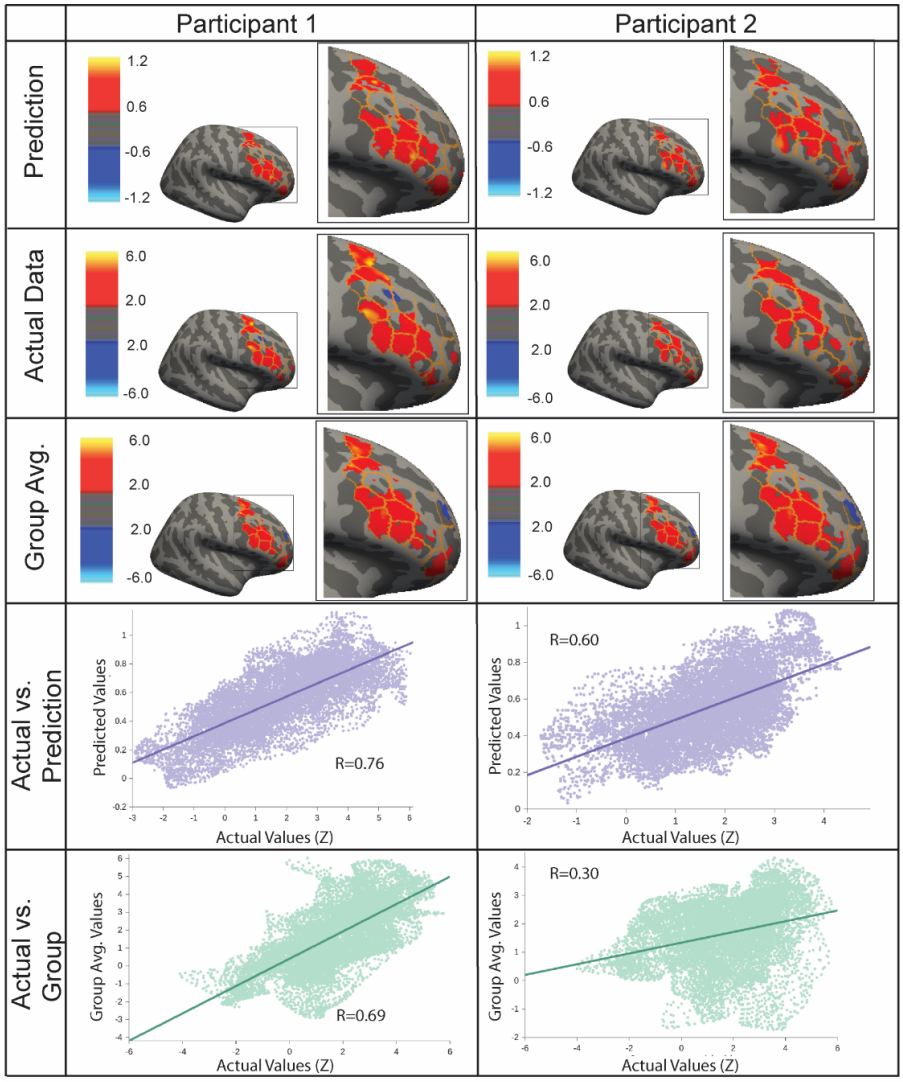
prediction performance value. Each of our three models' prediction performance values were then Fisher's z-transformed and used in a two-tailed paired t-test against the LOOGM benchmark to assess which model had the most accurate performance.

Although the ridge regression was employed to identify individual-participant activation, the nested LOOCV can still be influenced by large-scale similarities in the functional connectomes of the group. Further, as we know that individual participants may show more variable task activation, we wanted to test how much of this variability affected model performance. We calculated the extent to which a particular participant's task-activation was related to ridge performance in two ways. First, we took the absolute value of all participants' voxelwise activation data subtracted from the voxelwise group average data. We averaged this difference to get one value for each participant that signifies their deviation from the group average. This value was correlated with the z-transformed ridge performance values for each participant. We hypothesized that participants whose BOLD patterns were more similar to the group average would have better model performance. Next, we took the first level GLM z-statistics for each participant, for each run, and calculated a split-run metric of task activation reliability (Tripathi et al., 2024). For this analysis, we re-ran the FsFast GLMs to be calculated at the individual run level for each participant. The resulting z-statistics from the first three functional runs were averaged together and correlated with the z-statistics from the average of the last three runs for each participant. These correlation coefficients were then z-transformed and correlated with the ridge prediction performance values for all participants. We hypothesized that participants with higher BOLD reliability over the course of the scan

runs would result in more accurate model performance. Importantly, this metric defines a ceiling estimate for model performance, as task activation patterns contain noise. Understanding the reliability across runs within participants gives us an estimate of what our model should aim for in predicting task activation.

3. Results

Figure 3



Activation values comparing model prediction against the group. These activation plots show the predicted z-statistics from two example participants during Symbolic Reasoning - Symbolic Matching. In the top row are the model predictions using the CF method. Below that are each participants actual activation patterns within the search space. The third row depicts the group average results. Z-statistic ranges are plotted to the left of each surface-space brain image. The correlation between the participant's predicted and actual z-statistics are plotted in purple. The correlation between the group average and the participant's actual z-statistics are plotted in green.

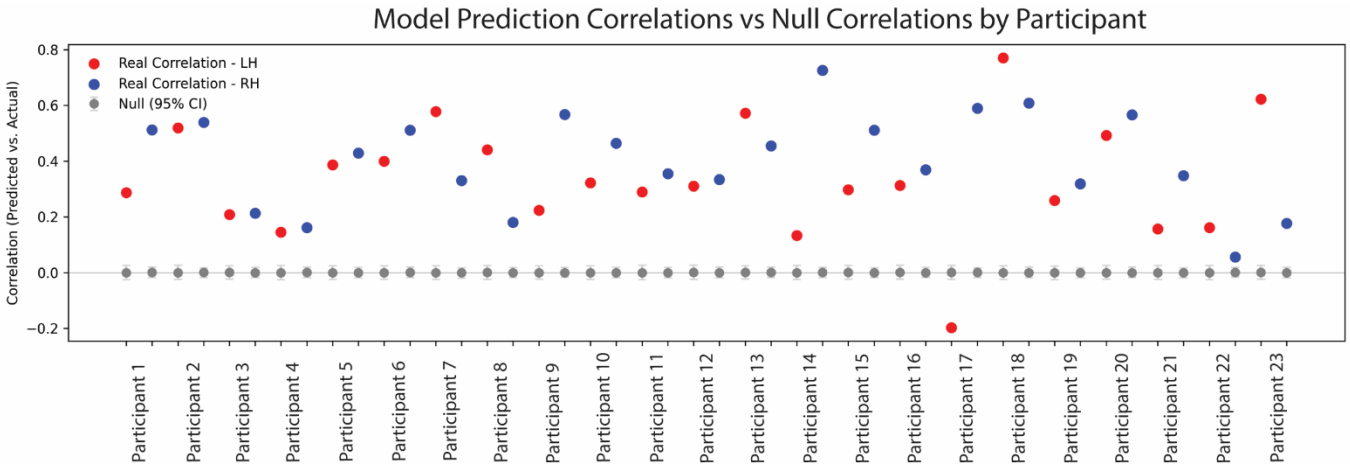
3.1 Whole-brain Ridge Prediction Performance

We used whole-brain functional connectomes from each hemisphere to create vertex-to-parcel connectivity matrices for each vertex in our search space (lateral PFC of the CCN). These connectomes were used to train a ridge regression model via a nested cross-validation procedure whereby the optimal parameters were generated on the basis of all n-2 inner loop participants and applied to the connectome of the left-out participant, resulting in predicted activation values for each hemisphere within the search space of each participant. Model performance was assessed via Pearson correlation between the participant-specific predicted search space values and their lower level voxelwise z-statistics. Model performance for each participant was also compared to their LOOGM generated z-statistics using paired, two-tailed t-tests. Whole-brain model predictions were moderately accurate for both the left and right hemisphere search spaces, and significantly more accurate than the group average predictions. Z-transformed performance for the whole-brain model was 0.37 and 0.45, compared to the group average at 0.30 and 0.38 in the lateral PFC of the left and right hemispheres respectively (left: $t(22)=2.11$, $p=0.04^*$, right: $t(22)=2.56$ $p=0.017^*$). Examples of two participant's model prediction activations, first level BOLD activations, and the group average are shown in **Figure**

3. Each participant's prediction vs. actual data and group average vs. actual data (Pearson's R correlation) are shown for comparison.

Our search space was small with robust group-level activation patterns throughout. Thus, it is possible that model performance is due to a wide spread of positive activation values throughout the search space, rather than spatially meaningful estimates. To test whether this was the case, we calculated null models by randomly permuting the predicted search space vertices 1000 times and calculating the correlation between each newly permuted distribution and the true vertex-wise values. Our results suggest that our model predictions are significantly

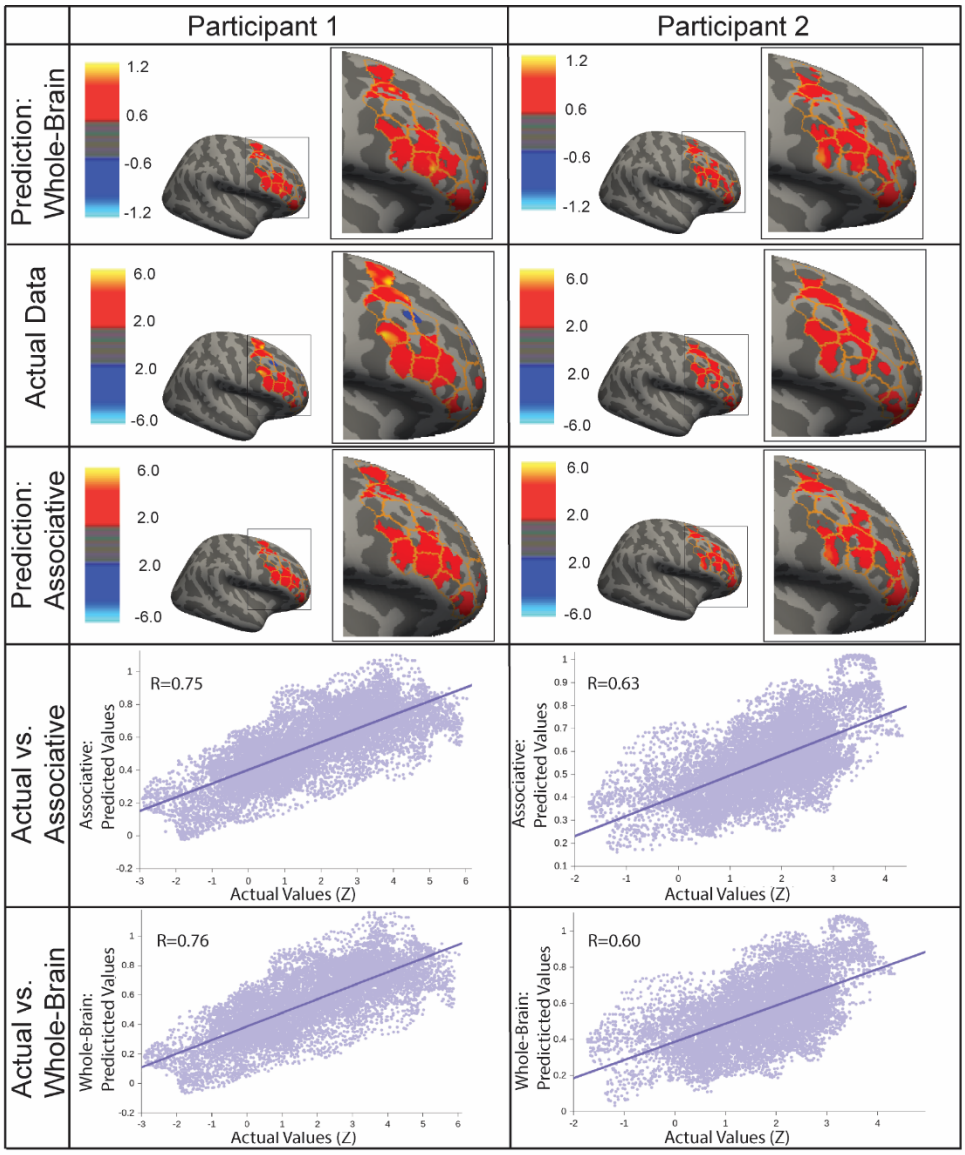
Figure 4



Model Predictions versus Permutated Null Correlations. For each participant, we randomly permuted the predicted values within their search space across 1000 permutations, calculating null model correlations for each permutation. The true model correlation for each hemisphere is plotted in red and blue (left and right hemispheres, respectively) and the null permutated correlations are plotted in gray.

greater than the shuffled null correlations across all participants (with the exception of one) in both hemispheres ($p<0.0001$ across all comparisons) (**Figure 4**).

Figure 5



Activation values comparing model predictions. These activation plots show the predicted z-statistics from two example participants during Symbolic Reasoning - Symbolic Matching. In the top row are the model predictions using the the whole-brain functional connectomes. Below that are each participants actual activation patterns within the search space. The third row depicts predictions using functional connectomes constructed using only the multimodal association networks. Z-statistic ranges are plotted to the left of each surface-space brain image. The correlation between each model's predictions and the participant's actual z-statistics are plotted in purple.

3.2 Sensory & Cognitive Connectome Ridge Prediction Accuracies

We next wanted to assess whether the whole-brain functional connectomes were necessary for model performance. As abstract reasoning elicits strong activation in frontoparietal brain regions (Melrose et al., 2018; Shin & Jeon, 2021), we hypothesized that connectivity between brain networks more involved in goal-directed attention and higher-order cognition would be better suited to predict task-evoked BOLD activation. We created two separate functional connectomes, one sensory connectome containing visual, limbic, and somatomotor network nodes, and one association connectome containing default mode, dorsal attention, ventral attention, and cognitive control network nodes. Separate ridge regressions trained on each of these connectomes were conducted using the same methods described above. We compared model performance of each model prediction outcome with one another and against the group average using paired two-tailed t-tests.

For the sensory connectome model, performance did not significantly differ from the group average in either of the hemispheric search spaces. Z-transformed performance was 0.32 and 0.41, compared to the group average at 0.30 and 0.38 in the left and right hemispheres respectively (ns). The association connectome model performance was moderate and significantly better than that of the group average at 0.37 and 0.46 in the left and right hemispheric search spaces respectively (left: $t(22)=2.12$, $p=0.04^{*}$, right: $t(22)=2.49$ $p=0.02^{*}$). Additionally, the associative model performance was significantly better than that of the sensory model performance for both hemispheres (left: $t(22)=3.40$, $p=0.003^{**}$, right: $t(22)=3.17$ $p=0.004^{**}$). Notably, model performance generated from the association connectome was not significantly different from that of our whole-brain connectome, suggesting that training the

358 model on connectivity matrices only from the cognitive control, dorsal attention, ventral
359 attention, and default mode networks is sufficient to predict task activation during symbolic
360 reasoning. Examples of two participant's associative model prediction activations, the whole-
361 brain ridge prediction activations, and the group average are plotted for comparison in **Figure**
362 **5.** We ran the same permutated null model comparison as reported above, and had nearly
363 identical findings such that all participants associative model performances (with the exception
364 of one) were significantly greater than the null model in both hemispheres. Comparisons
365 across participants can be seen in **Supplementary Figure 2. E**ach participant's whole-brain
366 ridge prediction vs. actual data and associative ridge prediction vs. actual data (Pearson's R
367 correlation) are provided for comparison. Performance averages of the different models are
368 shown as bar plots in **Figure 6.**

Figure 6



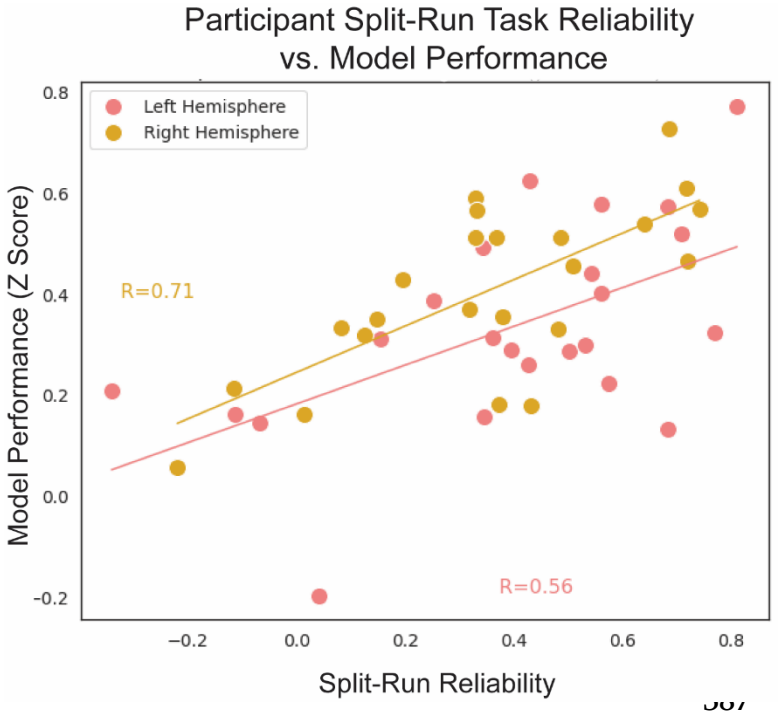
Model accuracies for comparison. Bar plots show the mean performance values for each model used in the analysis, for the right and left search spaces separately: whole-brain LOOCV, group average, associative LOOCV, and sensory LOOCV. Error bars represent the 95% confidence interval around the mean. * $p < 0.05$, ** $p<0.01$.

As an exploratory comparison, we also extracted whole-brain connectome model coefficients for each participant, averaged them, and plotted their average weights on inflated brains in both hemispheres. This served to assess which parcels contributed most to our whole-brain model predictions, and the level to which these overlapped with our split connectome models. Plotted coefficients are shown in **Supplementary Figure 1** and the top 40 weights are listed in descending order by parcel in **Supplementary Tables 1A & 1B.** The results demonstrate that in the right hemisphere, the strongest model coefficients come primarily from dorsal attention network, with some contributions from parietal regions in the cognitive control network, and temporal parietal regions of the ventral attention network. In the left hemisphere, dorsal attention network and temporal/parietal cognitive control network

provide the strongest model coefficients, with contributions from limbic networks as well. The whole-brain model coefficients share a large amount of overlap with our associative/sensory model splits, particularly with temporoparietal regions of the cognitive control and dorsal attention networks.

3.3 Participant Task Reliability and Ridge Model Performance

Figure 7



Participant variability versus ridge model performance. Correlation plot showing the relationship between a participant's run by run task activation reliability and their ridge performance. The higher the ridge performance, the more stable a participant's activation across scan runs.

Given our sample size, the parcellation scheme we chose, and individual variability, it is possible that the performance of our models was influenced by large-scale similarities between participants. As such, we wanted to assess how variability within an individual participant might influence model performance. Further, due to the inherent noise in fMRI data, we aimed to define a ceiling estimate for model performance. First, we correlated the extent to which an individual participant's task activation deviated from the group average with their model performance.

In both hemispheres we saw an overall trend where the larger the deviation of a participant's activation from the group average, the lower their model performance, however this was only significant in the right hemisphere (right: r=-0.49, p=0.016*, left: r=-0.33, p=0.1). We then took the average task activation across the first three functional runs for each individual participant and correlated it with their average task activation across the last three functional runs. This value was then correlated with their model performance. In both hemispheres, a participant's split-run activation reliability was significantly correlated with their task performance, suggesting that the less variable their activations were across runs, the more accurate their model prediction was (right: r=0.7, p=0.0002***, left: r=0.55, p=0.0062**) (**Figure 7**).

4. Discussion

Our study used connectome fingerprinting to predict BOLD activation in the lateral prefrontal cortex at the individual participant level during an abstract reasoning task. The results showed that CF can more accurately predict individual-level activation compared to the group average. Moreover, we demonstrated that we could accurately predict prefrontal brain activity using an "associative" subset of the full functional connectome for both hemispheric search spaces. Importantly, our results suggest that the underlying functional architecture of brain connectivity across these higher-order networks (the fingerprint) helps shape BOLD activation patterns during abstract reasoning.

4.1 Ridge Model Predictions on the Lateral Prefrontal Cortex

Consistent with previous studies, we found that CF can more accurately predict individual BOLD activation patterns compared to the group average (Osher et al., 2019; Tobyne et al., 2018; Tripathi et al., 2024; Tripathi & Somers, 2023). Hallmark studies by Osher et al. and Tobyne et al. were able to achieve impressive CF prediction of brain activity during salient directed attention tasks that elicited unique patterns of prefrontal activation at the individual level (Osher et al., 2019; Tobyne et al., 2018). Taking this model one step further by employing it during a range of cognitively demanding tasks, follow-up work from Tripathi & Somers used CF to predict BOLD activation in the cerebellum, where individual activation patterns were more variable. The goal of our study was to examine a more abstract form of higher-order cognition, abstract reasoning. Abstract reasoning relies on the lateral prefrontal cortex, a region with known inter-individual structural and function variability. By selecting a cognitive task known to activate a region with high inter-individual variability, we examined the potential link between individual-level activation patterns and the functional organization of the brain. Specifically, we aimed to assess the capacity of the CF method to capture this link during abstract, higher-order cognition. The model's success suggests that widely distributed brain networks involved in multi-modal demands contribute to BOLD activation patterns during abstract reasoning. These underlying distributed networks have far reaching implications in localized activation patterns during task performance. Thus, CF has useful implications for the analysis of more complex, higher-order cognitive tasks, and demonstrates that trait-specific information present at resting-state that is informative of state-level higher-order cognition.

436

437 *4.2 Split-connectome Prediction and the Link between Task-Based Activation patterns*

438 *and Inherent Resting-State Functional Connectivity*

439 Previous CF studies have demonstrated that individual brain activity patterns can be

440 identified using a subset of the entire functional connectome (Finn et al., 2015; Peña-Gómez

441 et al., 2018). For example, Finn et al. identified the frontoparietal network (i.e. CCN) as

442 containing the most important regions for accurate participant identification (2015).

443 Additionally, a recent study demonstrated the ability of CF to achieve a 98% accuracy rate in

444 identifying individual participants using only 0.3% of the whole connectome (Byrge &

445 Kennedy, 2019). These results suggest that individual task activation patterns can be predicted

446 from only a few connections within the functional connectome (Osher et al., 2019; Tobyne et

447 al., 2018).

448 To test how much of the whole-brain functional connectome is necessary for model

449 performance, our study split the connectivity matrices into two separate connectomes based

450 on overall network function. The first connectome was constructed with sensory specific

451 networks: the visual, somatomotor, and limbic networks. The second connectome was

452 constructed from higher-order association networks: the default mode, dorsal attention,

453 ventral attention, and cognitive control networks. We found that with the associative network

454 connectome, our model was able to achieve the same level of performance as the CF

455 constructed with the whole-brain connectome. This finding is supported by previous research

456 that found the default mode, dorsal attention, ventral attention, and cognitive control

networks contribute most strongly to the identification of individual functional connectomes (Peña-Gómez et al., 2018).

One reason for this could be the nature of a higher-order cognitive task, as these multi-model networks and their nodes have been implicated in higher-order cognition (Breedt et al., 2023; Morin et al., 2023; Murphy et al., 2020). Several modeling frameworks suggest that task activation is an emergent property of signal propagation through a scaffold defined by structural and functional connectivity (Bassett et al., 2018; Cole et al., 2019; Tavor et al., 2016). In fact, while resting-state connectivity is often described as a static measure, dynamic analyses suggest that the brain alters its connectivity structure throughout periods of rest. This allows us to capture evidence of efficiency and flexibility in the performance of higher-order cognition (Deng et al., 2022).

Alternatively, there could be an evolutionary role for tight coupling between the connectome and higher-order task activation patterns. In a recent paper linking the organization of the functional connectome to voxelwise activations across a broad array of cognitive domains, a robust connectivity-to-activation relationship was evident across the sample (Hiersche et al., 2026). Interestingly, they found the best fit by connectivity across higher-order cognitive domains related to memory, attention, and executive function, citing that perhaps this relationship reflects the ongoing strengthening of multi-modal brain regions through repeated activations and specialization across the lifespan (Hierche et al., 2026). Our results align nicely with this framework, as abstract reasoning is a specialized higher-order cognitive domain that develops in a prolonged manner across adolescence (Dumontheil, 2014).

Our results are consistent with the idea that the inherent connectivity features of these multi-modal networks at rest may hold information about higher-order cognition. In our case, while abstract reasoning requires strong activation of the prefrontal cognitive control network, resting-state connectivity of all multi-modal networks embeds this higher-order cognitive process. Thus, while higher-order cognition is often seen as state- or task-dependent, individual trait-level information within the functional connectome defines brain activity during cognitive tasks. Our CF model was able to capture this link with impressive performance, given within-participant variability in task activations of the lateral PFC.

4.3 Individual Variability and Task Reliability on Model Prediction

Prior work has highlighted cognitively meaningful individual differences in functional connectivity and task-based activation (Braga & Buckner, 2017; Frost & Goebel, 2012; Rademacher et al., 2001; Van Essen & Dierker, 2007), particularly in regions associated with higher-order cognitive functions (Braga & Buckner, 2017; Mueller et al., 2013). In a recent study where CF was used to predict motor activation in presurgical tumor patients, CF model performance was limited by the reliability of an individual's task activations across scan runs (Tripathi et al., 2024). Our results validate this finding by demonstrating that an individual's variability in task activation – both across runs and compared to the group average – was associated with the performance of the model's predictions. We found a robust positive correlation between split-scan run activation reliability and CF model performance, suggesting that model predictions tend to perform better in participants with higher cross-scan reliability. Given the inherent noise in fMRI data, even a perfect model performance could never reach a

correlation coefficient of 1. Therefore, these split-run correlation coefficients provide a ceiling for optimal model performance, as the model can only perform to the level of the participant's activation reliability across scans (e.g. our least reliable participants having the lowest model performance). We emphasize that our model performance was within impressive range when considering these ceiling estimates in both hemispheres. While we used random permuting of vertex-wise predicted values for our data analysis, we acknowledge that this could produce a relatively weak null as it does not retain the spatial autocorrelation of the data. Methods that incorporate spatial autocorrelation could provide a stronger test for future studies. Lastly, while we found a negative correlation between the deviation of an individual participant's activation from the group average and the CF model performance, it was only significant in the right hemisphere. This result can be interpreted in several ways. With our limited sample size this likely reflects higher stability and a better signal-to-noise ratio within participants and their canonical network structure. However, studies suggest that increasing sample size can lead to a decrease in model performance, suggesting a trade-off where a limited sample size can result in improved model performance (Li et al., 2021; Waller et al., 2017). Additionally, deviance from the group mean may also be reflective of biological variability, like arousal, which could also affect model performance.

During abstract reasoning, our results provide support that ridge regression-based connectome fingerprinting is better able to predict individual BOLD activity than the group average. A clear advantage of the connectome fingerprinting method is that less data is necessary for accurate model predictions. We provide evidence that a subset of association

networks performs as accurately as a model trained on the whole-brain connectome, thus identifying network nodes that made fundamental contributions to the model.

Data and Code Availability

Custom code used to generate the leave-one-out cross-validated model and carry out the aforementioned analyses is available via github at the following link: https://github.com/yixial-1736/connectome_fingerprint. All requests for de-identified data from the present manuscript will be made available upon request, subject to the review of the corresponding author and the Institutional Review Board at Boston University.

Author Contributions

Study design & conceptualization TMM, CES. Data acquisition: TMM. Data analysis: KI, YL. Writing: KI, YL, TMM, CES. Editing: KI, YL, TMM, CES.

Conflict of Interest

TMM has received consulting fees from Rocket Science Health. The other authors have no competing interests to declare.

Funding & Acknowledgements

This work was supported by the Office of Naval Research (grant numbers MURI N00014-16-1-2832, DURIP N00014-17-2304), and the National Science Foundation (grant number 1625552),

and the Boston University Kilachand Fund. The authors would like to acknowledge David Somers, Vaibhav Tripathi, and Harrison Fisher for helpful discussion on Connectome Fingerprinting Methods.

References

Amico, E., & Goñi, J. (2018). The quest for identifiability in human functional connectomes. *Scientific Reports*, *8*(1), 8254. https://doi.org/10.1038/s41598-018-25089-1

Amunts, K., Malikovic, A., Mohlberg, H., Schormann, T., & Zilles, K. (2000). Brodmann's Areas 17 and 18 Brought into Stereotaxic Space—Where and How Variable? *NeuroImage*, *11*(1), 66–84. https://doi.org/10.1006/nimg.1999.0516

Bassett, D. S., Zurn, P., & Gold, J. I. (2018). On the nature and use of models in network neuroscience. *Nature Reviews Neuroscience*, *19*(9), 566–578. https://doi.org/10.1038/s41583-018-0038-8

Braga, R. M., & Buckner, R. L. (2017). Parallel Interdigitated Distributed Networks within the Individual Estimated by Intrinsic Functional Connectivity. *Neuron*, *95*(2), 457-471.e5. https://doi.org/10.1016/j.neuron.2017.06.038

Breedt, L. C., Santos, F. A. N., Hillebrand, A., Reneman, L., van Rootselaar, A.-F., Schoonheim, M. M., Stam, C. J., Ticheler, A., Tijms, B. M., Veltman, D. J., Vriend, C., Wagenmakers, M. J., van Wingen, G. A., Geurts, J. J. G., Schrantee, A., & Douw, L. (2023). Multimodal multilayer network centrality relates to executive functioning. *Network Neuroscience*, *7*(1), 299–321. https://doi.org/10.1162/netn_a_00284

Buckner, R. L., & DiNicola, L. M. (2019). The brain's default network: updated anatomy, physiology and evolving insights. *Nature Reviews Neuroscience*, *20*(10), 593–608. https://doi.org/10.1038/s41583-019-0212-7

Bürgel, U., Amunts, K., Hoemke, L., Mohlberg, H., Gilsbach, J. M., & Zilles, K. (2006). White matter fiber tracts of the human brain: Three-dimensional mapping at microscopic resolution, topography and intersubject variability. *NeuroImage*, *29*(4), 1092–1105. https://doi.org/10.1016/j.neuroimage.2005.08.040

Byrge, L., & Kennedy, D. P. (2019). High-accuracy individual identification using a "thin slice" of the functional connectome. *Network Neuroscience*, *3*(2), 363–383. https://doi.org/10.1162/netn_a_00068

Chan, M. Y., Alhazmi, F. H., Park, D. C., Savalia, N. K., & Wig, G. S. (2017). Resting-State Network Topology Differentiates Task Signals across the Adult Life Span. *The Journal of Neuroscience*, *37*(10), 2734–2745. https://doi.org/10.1523/JNEUROSCI.2406-16.2017

Christoff, K., Prabhakaran, V., Dorfman, J., Zhao, Z., Kroger, J. K., Holyoak, K. J., & Gabrieli, J. D. E. (2001). Rostrolateral Prefrontal Cortex Involvement in Relational Integration during Reasoning. *NeuroImage*, *14*(5), 1136–1149. https://doi.org/10.1006/nimg.2001.0922

Cole, M. W., Bassett, D. S., Power, J. D., Braver, T. S., & Petersen, S. E. (2014). Intrinsic and Task-Evoked Network Architectures of the Human Brain. *Neuron*, *83*(1), 238–251. https://doi.org/10.1016/j.neuron.2014.05.014

Cole, M. W., Ito, T., Schultz, D., Mill, R., Chen, R., & Cocuzza, C. (2019). Task activations produce spurious but systematic inflation of task functional connectivity estimates. *NeuroImage*, *189*, 1–18. https://doi.org/10.1016/j.neuroimage.2018.12.054

584 Deng, S., Li, J., Thomas Yeo, B. T., & Gu, S. (2022). Control theory illustrates the energy
585 efficiency in the dynamic reconfiguration of functional connectivity. *Communications*
586 *Biology*, *5*(1), 295. https://doi.org/10.1038/s42003-022-03196-0
587 DiNicola, L. M., Sun, W., & Buckner, R. L. (2023). Side-by-side regions in dorsolateral
588 prefrontal cortex estimated within the individual respond differentially to domain-
589 specific and domain-flexible processes. *Journal of Neurophysiology*, *130*(6), 1602–1615.
590 https://doi.org/10.1152/jn.00277.2023
591 Esteban, O., Markiewicz, C. J., Blair, R. W., Moodie, C. A., Isik, A. I., Erramuzpe, A., Kent, J.
592 D., Goncalves, M., DuPre, E., Snyder, M., Oya, H., Ghosh, S. S., Wright, J., Durnez, J.,
593 Poldrack, R. A., & Gorgolewski, K. J. (2019). fMRIPrep: a robust preprocessing pipeline
594 for functional MRI. *Nature Methods*, *16*(1), 111–116. https://doi.org/10.1038/s41592-
595 018-0235-4
596 Finn, E. S., Shen, X., Scheinost, D., Rosenberg, M. D., Huang, J., Chun, M. M., Papademetris,
597 X., & Constable, R. T. (2015). Functional connectome fingerprinting: identifying
598 individuals using patterns of brain connectivity. *Nature Neuroscience*, *18*(11), 1664–
599 1671. https://doi.org/10.1038/nn.4135
600 Frost, M. A., & Goebel, R. (2012). Measuring structural–functional correspondence: Spatial
601 variability of specialised brain regions after macro-anatomical alignment. *NeuroImage*,
602 *59*(2), 1369–1381. https://doi.org/10.1016/j.neuroimage.2011.08.035
603 Golde, M., von Cramon, D. Y., & Schubotz, R. I. (2010). Differential role of anterior
604 prefrontal and premotor cortex in the processing of relational information. *NeuroImage*,
605 *49*(3), 2890–2900. https://doi.org/10.1016/j.neuroimage.2009.09.009
606 Gordon, E. M., Laumann, T. O., Gilmore, A. W., Newbold, D. J., Greene, D. J., Berg, J. J.,
607 Ortega, M., Hoyt-Drazen, C., Gratton, C., Sun, H., Hampton, J. M., Coalson, R. S.,
608 Nguyen, A. L., McDermott, K. B., Shimony, J. S., Snyder, A. Z., Schlaggar, B. L.,
609 Petersen, S. E., Nelson, S. M., & Dosenbach, N. U. F. (2017). Precision Functional
610 Mapping of Individual Human Brains. *Neuron*, *95*(4), 791-807.e7.
611 https://doi.org/10.1016/j.neuron.2017.07.011
612 Gratton, C., Laumann, T. O., Nielsen, A. N., Greene, D. J., Gordon, E. M., Gilmore, A. W.,
613 Nelson, S. M., Coalson, R. S., Snyder, A. Z., Schlaggar, B. L., Dosenbach, N. U. F., &
614 Petersen, S. E. (2018). Functional Brain Networks Are Dominated by Stable Group and
615 Individual Factors, Not Cognitive or Daily Variation. *Neuron*, *98*(2), 439-452.e5.
616 https://doi.org/10.1016/j.neuron.2018.03.035
617 Green, A. E., Kraemer, D. J. M., Fugelsang, J. A., Gray, J. R., & Dunbar, K. N. (2012). Neural
618 correlates of creativity in analogical reasoning. *Journal of Experimental Psychology:*
619 *Learning, Memory, and Cognition*, *38*(2), 264–272. https://doi.org/10.1037/a0025764
620 Gu, S., Pasqualetti, F., Cieslak, M., Telesford, Q. K., Yu, A. B., Kahn, A. E., Medaglia, J. D.,
621 Vettel, J. M., Miller, M. B., Grafton, S. T., & Bassett, D. S. (2015). Controllability of
622 structural brain networks. *Nature Communications*, *6*(1), 8414.
623 https://doi.org/10.1038/ncomms9414

Hasselmo, M. E., & Stern, C. E. (2018). A network model of behavioural performance in a rule learning task. *Philosophical Transactions of the Royal Society B: Biological Sciences*, *373*(1744), 20170275. https://doi.org/10.1098/rstb.2017.0275

Hearne, L. J., Mattingley, J. B., & Cocchi, L. (2016). Functional brain networks related to individual differences in human intelligence at rest. *Scientific Reports*, *6*(1), 32328. https://doi.org/10.1038/srep32328

Hoshi, E., Shima, K., & Tanji, J. (2000). Neuronal Activity in the Primate Prefrontal Cortex in the Process of Motor Selection Based on Two Behavioral Rules. *Journal of Neurophysiology*, *83*(4), 2355–2373. https://doi.org/10.1152/jn.2000.83.4.2355

Kraus, B. T., Perez, D., Ladwig, Z., Seitzman, B. A., Dworetsky, A., Petersen, S. E., & Gratton, C. (2021). Network variants are similar between task and rest states. *NeuroImage*, *229*, 117743. https://doi.org/10.1016/j.neuroimage.2021.117743

Li, K., Wisner, K., & Atluri, G. (2021). Feature selection framework for functional connectome fingerprinting. *Human Brain Mapping*, *42*(12), 3717–3732. https://doi.org/10.1002/hbm.25379

Liao, X., Vasilakos, A. V., & He, Y. (2017). Small-world human brain networks: Perspectives and challenges. *Neuroscience & Biobehavioral Reviews*, *77*, 286–300. https://doi.org/10.1016/j.neubiorev.2017.03.018

Mangin, J.-F., Rivière, D., Cachia, A., Duchesnay, E., Cointepas, Y., Papadopoulos-Orfanos, D., Scifo, P., Ochiai, T., Brunelle, F., & Régis, J. (2004). A framework to study the cortical folding patterns. *NeuroImage*, *23*, S129–S138. https://doi.org/10.1016/j.neuroimage.2004.07.019

Mansouri, F. A., Freedman, D. J., & Buckley, M. J. (2020). Emergence of abstract rules in the primate brain. *Nature Reviews Neuroscience*, *21*(11), 595–610. https://doi.org/10.1038/s41583-020-0364-5

Mars, R. B., Sotiropoulos, S. N., Passingham, R. E., Sallet, J., Verhagen, L., Khrapitchev, A. A., Sibson, N., & Jbabdi, S. (2018). Whole brain comparative anatomy using connectivity blueprints. *ELife*, *7*. https://doi.org/10.7554/eLife.35237

Mattar, M. G., Wymbs, N. F., Bock, A. S., Aguirre, G. K., Grafton, S. T., & Bassett, D. S. (2018). Predicting future learning from baseline network architecture. *NeuroImage*, *172*, 107–117. https://doi.org/10.1016/j.neuroimage.2018.01.037

Melrose, R. J., Jimenez, A. M., Riskin-Jones, H., Weissberger, G., Veliz, J., Hasratian, A. S., Wilkins, S., & Sultzer, D. L. (2018). Alterations to task positive and task negative networks during executive functioning in Mild Cognitive Impairment. *NeuroImage: Clinical*, *19*, 970–981. https://doi.org/10.1016/j.nicl.2018.06.014

Melrose, R. J., Poulin, R. M., & Stern, C. E. (2007). An fMRI investigation of the role of the basal ganglia in reasoning. *Brain Research*, *1142*, 146–158. https://doi.org/10.1016/j.brainres.2007.01.060

Miller, E. K., & Cohen, J. D. (2001). An Integrative Theory of Prefrontal Cortex Function. *Annual Review of Neuroscience*, *24*(1), 167–202. https://doi.org/10.1146/annurev.neuro.24.1.167

Molloy, M. F., Saygin, Z. M., & Osher, D. E. (2024). Predicting high-level visual areas in the absence of task fMRI. *Scientific Reports*, *14*(1), 11376. https://doi.org/10.1038/s41598-024-62098-9

Morin, T. M., Moore, K. N., Isenburg, K., Ma, W., & Stern, C. E. (2023). Functional reconfiguration of task-active frontoparietal control network facilitates abstract reasoning. *Cerebral Cortex*, *33*(10), 5761–5773. https://doi.org/10.1093/cercor/bhac457

Mueller, S., Wang, D., Fox, M. D., Yeo, B. T. T., Sepulcre, J., Sabuncu, M. R., Shafee, R., Lu, J., & Liu, H. (2013). Individual Variability in Functional Connectivity Architecture of the Human Brain. *Neuron*, *77*(3), 586–595. https://doi.org/10.1016/j.neuron.2012.12.028

Murphy, A. C., Bertolero, M. A., Papadopoulos, L., Lydon-Staley, D. M., & Bassett, D. S. (2020). Multimodal network dynamics underpinning working memory. *Nature Communications*, *11*(1), 3035. https://doi.org/10.1038/s41467-020-15541-0

Ooi, L. Q. R., Orban, C., Zhang, S., Nichols, T. E., Tan, T. W. K., Kong, R., Marek, S., Dosenbach, N. U. F., Laumann, T. O., Gordon, E. M., Yap, K. H., Ji, F., Chong, J. S. X., Chen, C., An, L., Franzmeier, N., Roemer-Cassiano, S. N., Hu, Q., Ren, J., … Jack, C. R. (2025). Longer scans boost prediction and cut costs in brain-wide association studies. *Nature*, *644*(8077), 731–740. https://doi.org/10.1038/s41586-025-09250-1

Osher, D. E., Brissenden, J. A., & Somers, D. C. (2019). Predicting an individual's dorsal attention network activity from functional connectivity fingerprints. *Journal of Neurophysiology*, *122*(1), 232–240. https://doi.org/10.1152/jn.00174.2019

Passingham, R. E., Stephan, K. E., & Kötter, R. (2002). The anatomical basis of functional localization in the cortex. *Nature Reviews Neuroscience*, *3*(8), 606–616. https://doi.org/10.1038/nrn893

Peña-Gómez, C., Avena-Koenigsberger, A., Sepulcre, J., & Sporns, O. (2018). Spatiotemporal Network Markers of Individual Variability in the Human Functional Connectome. *Cerebral Cortex*, *28*(8), 2922–2934. https://doi.org/10.1093/cercor/bhx170

Power, J. D., Cohen, A. L., Nelson, S. M., Wig, G. S., Barnes, K. A., Church, J. A., Vogel, A. C., Laumann, T. O., Miezin, F. M., Schlaggar, B. L., & Petersen, S. E. (2011). Functional Network Organization of the Human Brain. *Neuron*, *72*(4), 665–678. https://doi.org/10.1016/j.neuron.2011.09.006

Prabhakaran, V., Smith, J. A. L., Desmond, J. E., Glover, G. H., & Gabrieli, J. D. E. (1997). Neural Substrates of Fluid Reasoning: An fMRI Study of Neocortical Activation during Performance of the Raven's Progressive Matrices Test. *Cognitive Psychology*, *33*(1), 43–63. https://doi.org/10.1006/cogp.1997.0659

Rademacher, J., Morosan, P., Schormann, T., Schleicher, A., Werner, C., Freund, H.-J., & Zilles, K. (2001). Probabilistic Mapping and Volume Measurement of Human Primary Auditory Cortex. *NeuroImage*, *13*(4), 669–683. https://doi.org/10.1006/nimg.2000.0714

Rajkowska, G., & Goldman-Rakic, P. S. (1995). Cytoarchitectonic Definition of Prefrontal Areas in the Normal Human Cortex: II. Variability in Locations of Areas 9 and 46 and Relationship to the Talairach Coordinate System. *Cerebral Cortex*, *5*(4), 323–337. https://doi.org/10.1093/cercor/5.4.323

RAVEN, J. C. (1941). STANDARDIZATION OF PROGRESSIVE MATRICES, 1938. *British Journal of Medical Psychology*, *19*(1), 137–150. https://doi.org/10.1111/j.2044-8341.1941.tb00316.x

Rosenberg, M. D., Finn, E. S., Constable, R. T., & Chun, M. M. (2015). Predicting moment-to-moment attentional state. *NeuroImage*, *114*, 249–256. https://doi.org/10.1016/j.neuroimage.2015.03.032

Rosenberg, M. D., Finn, E. S., Scheinost, D., Papademetris, X., Shen, X., Constable, R. T., & Chun, M. M. (2016). A neuromarker of sustained attention from whole-brain functional connectivity. *Nature Neuroscience*, *19*(1), 165–171. https://doi.org/10.1038/nn.4179

Schaefer, A., Kong, R., Gordon, E. M., Laumann, T. O., Zuo, X.-N., Holmes, A. J., Eickhoff, S. B., & Yeo, B. T. T. (2018). Local-Global Parcellation of the Human Cerebral Cortex from Intrinsic Functional Connectivity MRI. *Cerebral Cortex*, *28*(9), 3095–3114. https://doi.org/10.1093/cercor/bhx179

Shen, X., Finn, E. S., Scheinost, D., Rosenberg, M. D., Chun, M. M., Papademetris, X., & Constable, R. T. (2017). Using connectome-based predictive modeling to predict individual behavior from brain connectivity. *Nature Protocols*, *12*(3), 506–518. https://doi.org/10.1038/nprot.2016.178

Shin, M., & Jeon, H.-A. (2021). A Cortical Surface-Based Meta-Analysis of Human Reasoning. *Cerebral Cortex*, *31*(12), 5497–5510. https://doi.org/10.1093/cercor/bhab174

Somers, D. C., Michalka, S. W., Tobyne, S. M., & Noyce, A. L. (2021). Individual subject approaches to mapping sensory-biased and multiple-demand regions in human frontal cortex. *Current Opinion in Behavioral Sciences*, *40*, 169–177. https://doi.org/10.1016/j.cobeha.2021.05.002

Specht, K. (2020). Current Challenges in Translational and Clinical fMRI and Future Directions. *Frontiers in Psychiatry*, *10*. https://doi.org/10.3389/fpsyt.2019.00924

Tavor, I., Jones, O. P., Mars, R. B., Smith, S. M., Behrens, T. E., & Jbabdi, S. (2016). Task-free MRI predicts individual differences in brain activity during task performance. *Science*, *352*(6282), 216–220. https://doi.org/10.1126/science.aad8127

Thomas Yeo, B. T., Krienen, F. M., Sepulcre, J., Sabuncu, M. R., Lashkari, D., Hollinshead, M., Roffman, J. L., Smoller, J. W., Zöllei, L., Polimeni, J. R., Fischl, B., Liu, H., & Buckner, R. L. (2011). The organization of the human cerebral cortex estimated by intrinsic functional connectivity. *Journal of Neurophysiology*, *106*(3), 1125–1165. https://doi.org/10.1152/jn.00338.2011

Tobyne, S. M., Somers, D. C., Brissenden, J. A., Michalka, S. W., Noyce, A. L., & Osher, D. E. (2018). Prediction of individualized task activation in sensory modality-selective frontal cortex with 'connectome fingerprinting.' *NeuroImage*, *183*, 173–185. https://doi.org/10.1016/j.neuroimage.2018.08.007

Tripathi, V., Rigolo, L., Bracken, B. K., Galvin, C. P., Golby, A. J., Tie, Y., & Somers, D. C. (2024). Utilizing connectome fingerprinting functional <scp>MRI</scp> models for motor activity prediction in presurgical planning: A feasibility study. *Human Brain Mapping*, *45*(10). https://doi.org/10.1002/hbm.26764

Tripathi, V., & Somers, D. C. (2023). Predicting an individual's cerebellar activity from functional connectivity fingerprints. *NeuroImage*, *281*, 120360. https://doi.org/10.1016/j.neuroimage.2023.120360

Van Essen, D. C., & Dierker, D. L. (2007). Surface-Based and Probabilistic Atlases of Primate Cerebral Cortex. *Neuron*, *56*(2), 209–225. https://doi.org/10.1016/j.neuron.2007.10.015

Waller, L., Walter, H., Kruschwitz, J. D., Reuter, L., Müller, S., Erk, S., & Veer, I. M. (2017). Evaluating the replicability, specificity, and generalizability of connectome fingerprints. *NeuroImage*, *158*, 371–377. https://doi.org/10.1016/j.neuroimage.2017.07.016

Wallis, J. D., Anderson, K. C., & Miller, E. K. (2001). Single neurons in prefrontal cortex encode abstract rules. *Nature*, *411*(6840), 953–956. https://doi.org/10.1038/35082081

Welvaert, M., & Rosseel, Y. (2013). On the Definition of Signal-To-Noise Ratio and Contrast-To-Noise Ratio for fMRI Data. *PLoS ONE*, *8*(11), e77089. https://doi.org/10.1371/journal.pone.0077089